Long-term prediction of ground movement in expansive clays due to soil-atmosphere-vegetation interaction

J. Botha[1], C. W. MacMinn[1], H. J. Burd[1], and S. Acikgoz[1],

[1]*Department of Engineering Science, University of Oxford, Oxford, United Kingdom, email: janet.botha@eng.ox.ac.uk*

ABSTRACT

Expansive clays undergo large volume changes due to variations in water content, leading to ground subsidence and/or heave. These variations are driven by weather and other environmental factors, like vegetation. Globally, expansive clays are considered a geohazard that is responsible for extensive financial loss due to adverse impacts on lightweight, shallow infrastructure. Low-rise masonry buildings – including many historical structures – have limited tensile strength, making them particularly vulnerable to structural damage and instability arising from differential ground movement. To date, assessment of the risk of damage to masonry buildings situated on expansive clays has relied on a simplified, uncoupled approach that predicts ground movement by simulating groundwater flow in rigid soil and then converting the resulting suctions to displacements through empirical relations. Although useful for preliminary assessment, this approach overlooks the soil-atmosphere-vegetation interactions and coupled hydro-mechanical behaviour of unsaturated soil. Here, a new model is developed to conduct hydro-mechanical analysis of variably saturated elastic soil to simulate swelling and shrinkage in response to tree water uptake and evapotranspiration. In addition to assessing risk, this model can also be used to inform interventions to control tree-related ground movement near existing masonry buildings. The capabilities of the model are illustrated by simulating the initial localised desiccation of a site with elm trees, and the subsequent heave that occurred a year following tree removal and construction. This preliminary analysis does not consider building loading and stiffness, accounting for construction only through changes in the hydraulic boundary conditions; future work will include coupled soil-structure interaction.

Keywords: Expansive clays, subsidence, heave, soil-atmosphere-vegetation interaction, numerical modelling, coupled flow-deformation

INTRODUCTION

Ground subsidence and heave, from clay shrinkage and swelling, respectively, are caused by changes in soil water content due to changes in climate and vegetation. Expansive clays tend to shrink or swell because of the constituent active clay minerals that adsorb and retain large quantities of water in an exchangeable state (Norrish, 1954; Reeve et al., 1980; Jones et al., 2020). The zone or depth of the soil, below ground level, that experiences this volume change is termed the 'active zone' and has been reported to range between 1.5 and 4.0 m; were areas with highly expansive clay were observed to have a deeper active zone (Biddle, 2001; Nelson et al., 2001) . Lightweight infrastructure founded on shallow ground can sustain damage when subjected to ground movement, including cracking, distortion, and instability – with severity depending on the magnitude of movement and vulnerability of the structure (Driscoll, 1983). Low-rise masonry structures such as residential buildings are particularly susceptible because of their limited tensile strength.

Vegetation exacerbates differential movement through localised effects. Trees can create extremely dry regions in the soil, causing shrinkage. Similarly, tree removal can trigger re-saturation in a dry zone, causing heave. Due to the nature of weather and tree water uptake, shrinkage and swelling is typically cyclic, corresponding to dry and wetter conditions or active growing and dormant seasons respectively. However, extreme weather or changes in environmental conditions can result in unprecedented magnitudes of movement and building damage. For example, the 1990–1992 droughts in the UK resulted in a surge of insurance claims related to subsidence damage (Crilly, 2001; Murphy et al., 2020). Subsidence and heave can occur over long timescales, from years to decades. Numerical modelling is useful in these scenarios to simulate the ground and structure for the assessment of risk and mitigation strategies. It can also be used to improve current knowledge on the critical conditions and mechanisms that result in ground movement and associated building damage.

Soil-atmosphere-vegetation interaction comprises several physical phenomena, including infiltration, evaporation, tree water uptake, and variably saturated groundwater flow and deformation. Although each phenomenon is individually well researched, with advanced numerical modelling strategies, there have been few attempts to create comprehensive models that capture all of them in a single model for the prediction of ground movement in expansive soils to assess building damage risk. For example, Vrugt et al. (2001) modelled three-dimensional water uptake in a rigid soil around a tree, while El-Garhy and Wray (2006) predicted ground movements using an uncoupled approach where groundwater flow and deformation were modelled separately. This paper presents a concise formulation of a new soil-atmosphere-vegetation interaction model and illustrates its use in predicting long-term changes in soil moisture content and deformation using a case study. The case study also demonstrates how the model can be used to inform interventions for existing masonry structures affected by vegetation-related subsidence or heave. Such interventions have historically relied on qualitative assessments and judgement from arboriculturists. The ability to simulate tree removal, planting, and pruning to assess the soil's hydromechanical response allows a more detailed and quantitative assessment of different interventions.

METHODOLOGY

Coupled flow-deformation formulation

A dual-porosity conceptual model is adopted to describe the structure of active clays, similar to work by Alonso et al. (1999), and Wang and Wei (2015). The soil is assumed to comprise macro and micro pores, such that majority of the flux occurs in the macro pores while the micro pores hold immobile/swelling water. The formulation allows for unsaturated-saturated flow in a deformable, swelling soil, and plant water uptake. The following sign convention is used: tensile stresses are positive, such that pore water and air pressure correspond to negative (compressive) stresses, and the vertical z axis is positive upwards.

We assume that the air phase is passive, so that the pore air pressure, p_a, is fixed and equal to atmospheric pressure, which we take to be zero. Thus, the pore water pressure, p_w, is positive only in the saturated zone. The matric suction, p_c, is the difference between the air pressure and the water pressure,

$$p_c = p_a - p_w, \tag{1}$$

which is extended to capture both saturated and unsaturated regions via (Chung & Austin, 1987; Mathias, 2023)

$$p_c = \begin{cases} 0 & if\ p_w \geq 0 \\ -p_w & if\ p_w < 0 \end{cases}. \tag{2}$$

Conservation of mass for the pore water in the two structural levels considering an Eulerian reference frame is

$$\frac{\partial}{\partial t}(\theta_M \rho_w) + \nabla \cdot Q_w + \Omega \rho_w = -\Gamma \tag{3}$$

and

$$\frac{\partial}{\partial t}(\theta_m \rho_w) = \Gamma, \tag{4}$$

where θ_M and θ_m are the macro and micro volumetric water content with respect to the total volume, respectively, ρ_w is the density of water, Γ is the mass rate of water exchange between the two pore networks, Ω is the volume rate of root water uptake (RWU), and Q_w is the mass flux of water through the pore space. Darcy's law is adopted to relate Q_w to p_w in the standard way. Alonso and Navarro (2005) proposed the following linear relation for Γ:

$$\Gamma = \eta\,(\mu_M - \mu_m), \tag{5}$$

where μ_M and μ_m are the chemical potential of the pore water in the macro and micro pores, respectively, and η controls the rate of mass exchange. The expressions for μ_M and μ_m provided by Alonso and Navarro (2005) are functions of the mean confining stress and the salinity; thus, their approach does not assume mechanical, hydraulic, and chemical equilibrium between the two structural levels. The macroscopic approach by Vrugt et al. (2001) for the formulation of the rate of RWU, Ω, is adopted. It assumes uniform RWU in each representative elementary volume and therefore can consider any spatial distribution of roots. The groundwater flow formulation requires two additional constitutive relations: a soil-water retention function and a relative permeability function. The retention function describes the relationship between water content and suction, while the relative permeability function relates the macrostructural degree of saturation, S_M, to ease of water flow. The retention and permeability functions proposed by van Genuchten (1980) are adopted. To achieve continuity of flow between the saturated and unsaturated regions, weak compressibility of the pore water is assumed (Chung & Austin, 1987; Mathias, 2023). The water in the micropores is held tightly to the clay particles by capillary and other physicochemical forces, so the microstructure is assumed to be saturated, thus taking the microstructural degree of saturation S_m to be equal to one. Equation 1–5 and the referenced constitutive models constitute the groundwater flow module capable of simulating saturated-unsaturated groundwater flow and RWU.

Momentum conservation in three dimensions, neglecting inertial forces, is

$$\nabla \cdot \sigma + b = 0, \tag{6}$$

where σ is the total Cauchy stress and b is the body force. We adopt Bishop's effective stress σ' for the average skeleton stress in a partially saturated soil,

$$\sigma' = \sigma + [p_w + p_c(1 - S_M)]I, \tag{7}$$

where I is the identity tensor. Bishop's formulation reduces to Terzaghi's effective stress when the macrostructure is saturated, $S_M = 1$. The total porosity ϕ measures the volume of voids per unit total volume. Similarly, the macro porosity ϕ_M and the micro porosity ϕ_m measure the volumes of macro voids per unit total volume and micro voids per unit total volume, respectively, and $\phi = \phi_M + \phi_m$. The total volumetric strain ε_v is assumed to comprise a macro component ε_v^M and a micro component ε_v^m,

$$\varepsilon_v = \varepsilon_v^M + \varepsilon_v^m, \tag{8}$$

with

$$\varepsilon_v^M = \frac{\Delta\phi_M}{1-\phi_0} \tag{9}$$

and

$$\varepsilon_v^m = \frac{\Delta\phi_m}{1-\phi_0}, \tag{10}$$

with ϕ_0 the initial porosity. Small deformations are assumed, such that ε_v can also be calculated using the standard strain-displacement relations. The micro-scale strain ε_v^m accounts for aggregate deformation due to the physicochemical processes taking place between the pore water and clay minerals, while the macro-scale strain ε_v^M accounts for the deformation of the macrostructure due to mechanical loading and suction. Wang and Wei (2015) postulated that volumetric strains in the microstructure are mostly reversible, while those in the macrostructure are irreversible. Cyclic wetting and drying tests have shown that irreversible volumetric strains are accumulated during the first few cycles and are attributed to particle rearrangement and aggregate disintegration. Subsequently, any further swelling and shrinkage can be considered elastic, occurring predominantly due to deformation of the microstructure (Nowamooz et al., 2009). A linear elastic constitutive model is adopted for both the macro and microstructure. Therefore, the model cannot reproduce irreversible macrostructural deformation, which can lead to underestimation of both shrinkage and swelling strains. However, the irreversible strains are expected to be small compared to the reversible strains as demonstrated by Wang and Wei (2015). The macrostructural constitutive model is standard linear elasticity, which in this case relates Bishop's effective stress to macrostructural strain. The microstructural constitutive model used here is that of Navarro et al. (2015),

$$e_m = -\kappa_m \ln\left(\frac{p_{cm}}{p_{cm}^*}\right), \tag{11}$$

where e_m is the microstructural void ratio, p_{cm} is the microstructural suction, and p_{cm}^* is the microstructural suction at the dry state, taken here to be $p_{cm}^* = 10^6$ Pa. e_m is related to ϕ_m through standard volume relations.

The model equations are solved using MATLAB's ODE15s, an implicit solver for stiff initial-value problems and differential-algebraic systems. The spatial derivatives are approximated with staggered, second-order finite-difference formulas to convert the governing partial differential equations into a system of coupled ODEs in time (i.e., the method of lines). The resulting semi-discrete system is then amenable to integration with ODE15s. The two-dimensional form of the model is used for the analyses below (i.e., plane flow and plane strain).

Problem description and model setup

The case study considered here relates to Queens Gate Cottages (Windsor Great Park, UK), a single-storey terraced masonry building on London clay that sustained damage from differential ground heave over a period of 32 years. The structure was constructed on a site where 1 or 2 elm trees, about 21 m tall, were felled prior to construction (Cheney, 1988). The trees are believed to have been very close to the building on the west end, near levelling station H in Figure 1, and would have locally desiccated the soil near one corner of the building. Re-saturation of the soil after construction caused a maximum differential heave of about 139 mm over 32 years. Figure 1 shows the building footprint, highlighting its dimensions and the inferred location of the trees based on the displacements measured by Cheney (1988), as well as the inferred radial zone of influence of the tree in terms of RWU. Façade FJ experienced the largest differential movement. The analysis simulates the ground below this façade.

Two analyses were conducted. The first simulates RWU in the year prior to construction to establish the initial desiccated state of the soil. This initial phase (IP) is then used as the initial condition for the main analysis (MA) to simulate heave in the first year after construction. The IP was modelled via a flow-only axisymmetric analysis from 1st January 1952 to 31st December 1952, with RWU only active during the growing season between March and August (dormant between September and February). A 35 m by 4 m domain was used for the IP, with the tree centred at the symmetry axis (Figure 2, left). The radial dimension of the domain was informed by the radial zone of influence of the tree, which is taken to be 1.5 times the mature tree height (i.e., 31.5 m). The rooted zone was therefore 31.5 m times 3.0 m, were

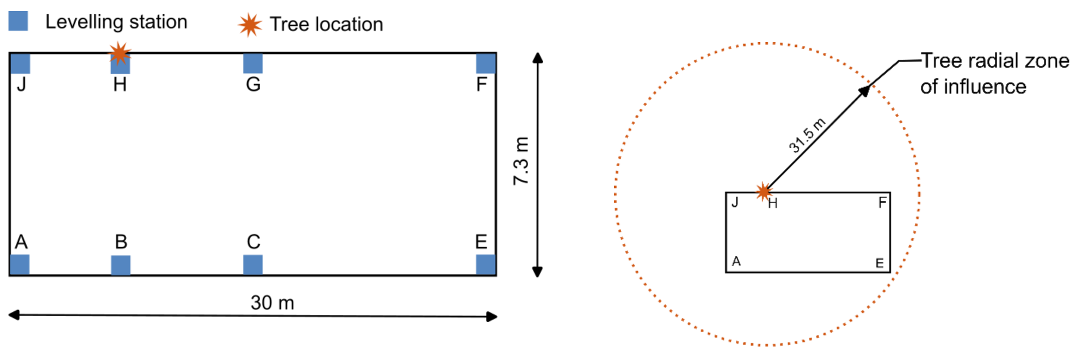

Figure 1. *Plan view of the building footprint, assumed tree location, and levelling stations modified from Cheney (1988) (left). Illustration of the building footprint in relation to the tree's inferred radial zone of influence (right).*

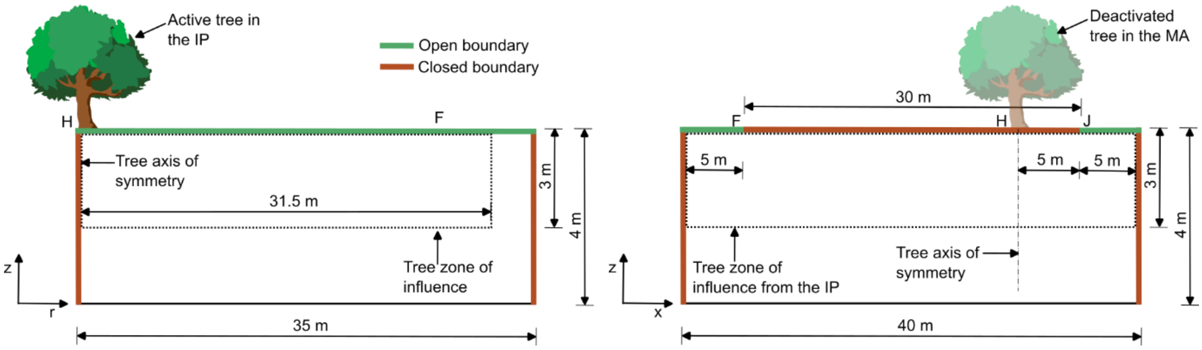

Figure 2. *Model set-up and boundary conditions for the initial phase (IP, left) and the main analysis (MA, right).*

Table 1. *Vrugt root water uptake (RWU) spatial distribution parameters*

z_m [m]	r_m [m]	p_z [-]	p_r [-]	z^* [m]	r^* [m]
3.0	31.5	1.0	1.0	0	0

3.0 m refers to the maximum rooting depth. The 1.5H rule and 3.0 m rooting depth is based on Biddle's (1983) measurements of water content near high-water-demand poplar trees. A 1.0H rule was historically used for all trees, but Biddle (1983) found that high-water-demand trees had larger zones of influence. Actual rooting distance are highly variable, depending on tree water demand, soil density, aeration, and water content. Table 1 lists the parameters used for the Vrugt RWU spatial distribution function, which are uniform within the rooted zone. The resulting RWU distribution decreases radially and vertically away from the trees. The elm trees are assumed to have a combined total potential transpiration rate of T_p = 1.5 m^3/day. This total is approximated from single-tree water-use estimates reported by Wullschleger et al. (1998). Actual RWU can be lower than T_p due to limited water availability. The model accounts for this constraint using the water-stress factor of Feddes et al. (1976).

The MA uses a 40 m by 4 m domain covering the full length of façade FJ and simulates the site from 1st August 1952 to 31st December 1953 (Figure 2, right). Removal of the tree and construction of the building are implemented by deactivating RWU and making the ground surface beneath façade FJ impermeable. Load and stiffness effects from the building are neglected. The following boundary conditions are prescribed. In the IP, the vertical side boundaries were closed for flow, while evaporative and infiltrative fluxes were imposed at the open top boundary. In both analyses, a fixed water table was assumed to exist at a depth of 7 m below ground level. This water table was enforced indirectly by imposing a fixed pore pressure of -10kPa at the bottom of the model, corresponding to the gravity-capillary equilibrium pore pressure at an elevation of 3 m above the water table (i.e., at a depth of 4 m). The hydraulic boundary conditions for the MA are the same, except that the ground surface beneath façade FJ is now taken to be impermeable. For the MA, these hydraulic boundary conditions are paired with the following mechanical boundary conditions: a fixed base, roller constraints on the vertical side boundaries, and a free top boundary.

Review of borehole logs near the study site from the British Geological Survey database supports Cheney's (1988) description of a 15 m layer of London Clay overlying Reading Beds. Table 2 shows the soil hydraulic and mechanical properties used. The adopted saturated permeability k_{sat} is higher than what is generally reported for clays. However, permeability is known to vary significantly with depth in shallow ground. For example, Dixon et al. (2019) measured permeability in the top 1 m layer of a London clay embankment and reported a range between 1 × 10^{-5} and 1 × 10^{-10}. This variability can be attributed to cracking of the clay under shrinkage. Figure 3 shows daily weather data near the site from the 1 km by 1 km resolution HadUK-Grid dataset (Met Office et al., 2018), which is used in the IP to determine the infiltration and evaporation fluxes at the open top boundary. Evaporation from bare soil is approximated using minimum and maximum air temperatures $T_{a,min}$ and $T_{a,max}$, respectively, following the aerodynamic approach by Mahfouf and Noilhan (1991), while total daily precipitation p_r is converted to a daily flux.

Table 2. *Soil hydraulic and mechanical properties*

k_{sat} [m/s]	α^a [Pa^{-1}]	n^a [-]	G^b [Pa]	v^b [-]	ρ_s [kg/m^3]	κ_m [-]	η [ms/kg]
1×10^{-6}	1×10^{-5}	1.56	2.25×10^6	0.33	2650	0.01	1×10^{-14}

[a] van Genuchten soil water retention and relative permeability parameters
[b] Macrostructural mechanical properties (G is the shear modulus and v is the Poisson ratio).

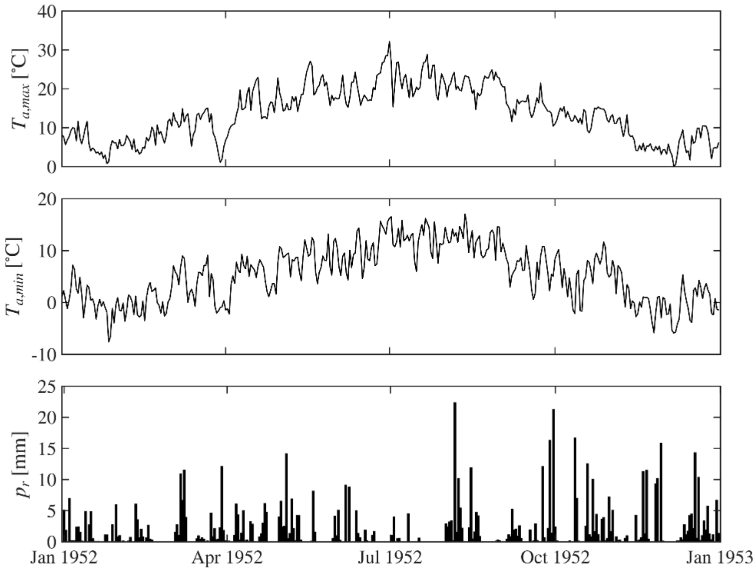

Figure 3. *Measured maximum and minimum air temperature (top and middle, respectively) and precipitation (bottom) used to approximate evaporative and infiltrative fluxes at the soil-atmosphere boundary during the IP analysis. Data courtesy of the Met Office (2018).*

RESULTS AND DISCUSSION

Figures 4 and 5 show the spatial distributions of pore water pressure and volumetric water content at two times during the IP and the MA, respectively. In Figure 4, r is the distance from the origin (i.e., the tree) in the axisymmetric IP. In Figure 5, x is the distance from the left edge of the rectangular domain. The August profiles for the IP are representative of the driest conditions, corresponding to summer and the end of the tree's active season. Conversely, the December profiles are representative of wetter conditions, following recharge during autumn and winter. The localised desiccation caused by RWU is reproduced by the model and clearly evident in the August profiles. The majority of the desiccation is near the tree, as should be expected from the adopted root distribution pattern, which decreases radially and vertically with distance away from the tree.

The RWU distribution has a significant influence on the desiccation profiles shown in Figure 4. Although the adopted RWU distribution has been observed for several species under normal soil conditions and relatively uniform water recharge (Biddle, 1983), there are exceptions. For example, in nonuniform recharge conditions such as a leaking drain, the spatial distribution of RWU can be concentrated around the drain, deviating from the assumption of water uptake being concentrated near the tree. Where water content data around a tree is readily available, it can be used to calibrate the RWU distribution parameters in Table 1, which can result in more accurate numerical predictions. However, due to the temporal variability of RWU, which is associated with growing seasons and weather, it is not apparent whether use of calibrated parameters will be superior in comparison with the standard spatial distribution in long term predictions since both approaches assume the RWU distribution is constant in time.

The difference in pore pressure and water content between August and December 1952 in Figure 4 highlights the transient hydraulic state in the shallow ground under the influence of atmospheric and vegetation effects. Since daily infiltration and evaporation were enforced at the soil-atmosphere boundary, the soil's transient hydraulic state was captured in good detail. The August pressure

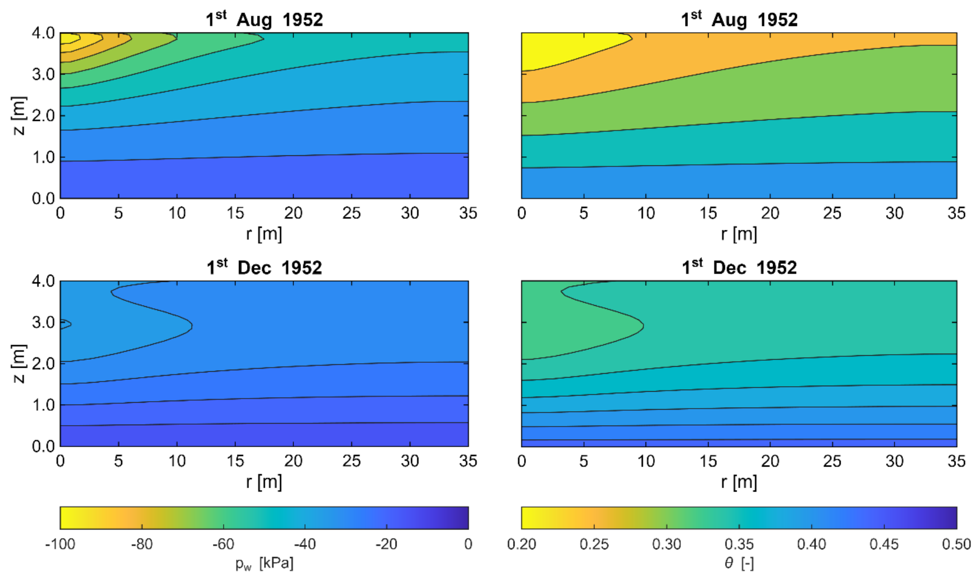

Figure 4. *Contours of pore pressure (left) and volumetric water content (right) for the IP analysis at the end of the dry season in August and following re-saturation in December. The active tree was located at r = 0 m, and z = 4.0 m.*

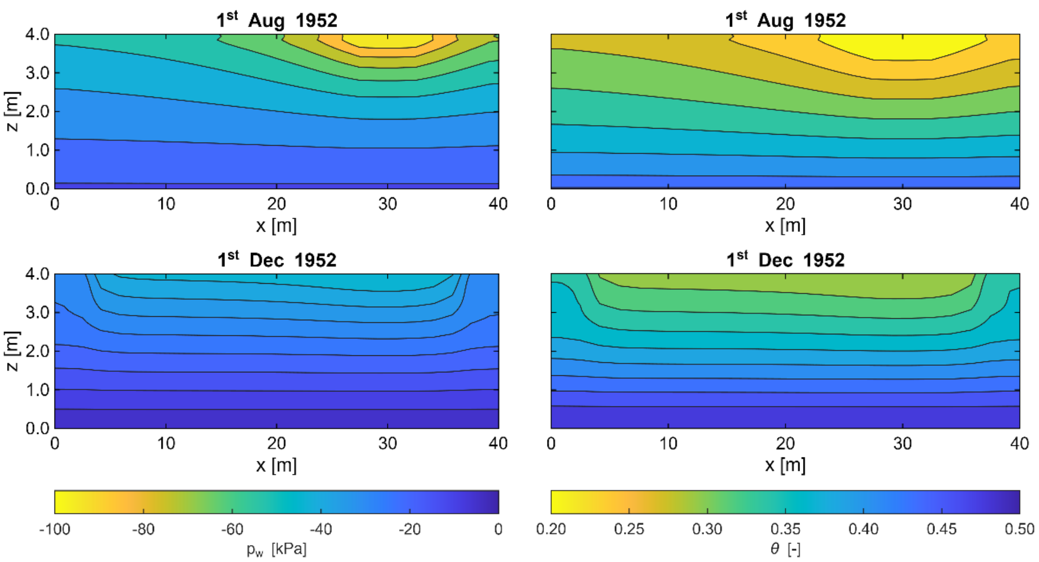

Figure 5. *Contours of pore pressure (left) and volumetric water content (right) for the MA at the end of the dry season in August and following re-saturation in December. The felled tree was located at x = 30 m and z = 4.0 m.*

distribution in Figure 4 was then used as the initial state for the MA, effectively assuming the tree was cut down in August 1952 and the building immediately constructed; such that the ground below wall FJ became impermeable (Figure 2, right).

The August results in Figure 5 are the initial state for the MA, constructed using the axisymmetric groundwater-flow results from August 1952 from the IP. This reconstruction assumes that the tree was located at x = 30 m and z = 4 m. Infiltration between August and December 1952 increases the water content in the soil, replenishing the desiccated soil near the tree. The wetting front can be seen in the December 1952 water content profile, which shows slightly higher water content below the top open boundaries than below the closed boundary. The December 1952 results in Figure 5 show that changing the hydraulic conditions at the site creates a drier zone below the façade when compared to the December 1952 results in Figure 4. Both the IP and the MA assume that the groundwater condition is constant throughout the analysis (i.e., that the water table is fixed at 7 m below ground level).

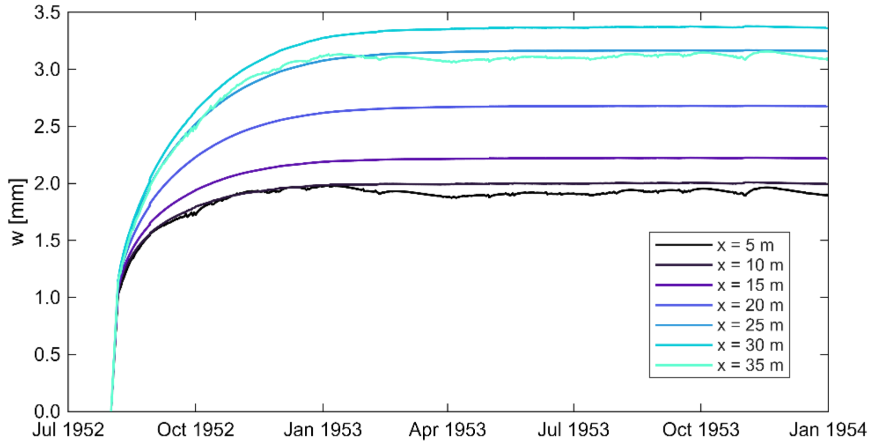

Figure 6. *Time evolution of predicted vertical displacement at select points on the ground surface between 1st August 1952 and 31st December 1953. The felled tree was located at x = 30 m.*

This water table elevation was inferred from reviewing bore hole logs and topography around the site in relation to the closest rivers. Although seasonal fluctuations in groundwater conditions are expected to affect the results, the impact would be mitigated by the 3 m elevation gap between the active zone and the average water table elevation used. For sites where the water table is shallow enough to supply trees with water directly, seasonal groundwater fluctuations will have a greater impact on the prevailing soil conditions.

Figure 6 shows the evolution of displacement at select points on the ground surface along façade FJ. The model correctly captures the swelling trend observed by Cheney (1988), with displacements initially increasing linearly with time and eventually plateauing. However, the magnitude of swelling displacement after one year is underpredicted. Cheney (1988) deduced a maximum swell of 10 mm near the tree one year after construction, while the numerical prediction shows a maximum swell of only 3.36 mm. The underprediction of displacement can be related to the high uniform permeability used in this analysis having prevented the generation of deep desiccation near the tree. A drier initial state for the MA, with higher suctions, would produce larger swelling deformation. However, the combination of low permeability, high suction, and a dynamic soil-atmosphere boundary condition exacerbates the numerical stiffness of this problem, resulting in convergence failure. A more realistic analysis of the problem using lower permeability requires a review of numerical techniques that can improve numerical robustness. The Darcy flux during the MA was predominantly vertical, along with some horizontal flow re-saturating the soil beneath wall FJ. This highlighted the potential dependency of the resulting hydraulic and deformed state on the dominant mechanism driving water flow across the domain: gravity, capillary forces, and inter-structural physicochemical forces.

CONCLUSIONS

A new numerical model for the simulation of coupled soil-atmosphere-vegetation interaction is presented. The model includes coupled hydro-mechanical analysis of variably saturated soil, swelling and shrinkage of expansive clays, tree root water uptake, and soil-atmosphere interaction. It was developed for the assessment of damage risk to low-rise masonry structures founded on expansive clays. It can also be used to inform mitigative interventions such as tree planting, removal or pruning, near existing masonry structures to control vegetation-related ground movement. The model is used to predict long-term ground movement at a site in Windsor, UK, where a single-storey masonry building incurred damage due to differential heave over 32 years post construction. The site was desiccated by elm trees, which were removed just before construction. This preliminary analysis did not consider building loading and stiffness, accounting for construction at the site by changing only the hydraulic boundary conditions. The model has reproduced the trends concerning localised desiccation in the soil around the trees, and the transient pore water pressure and water content due to weather conditions. In the analysis of the site post construction of the building, the model captures the observed swelling trend, were displacements initially increase linearly with time and eventually plateau. However, the model underpredicted the magnitude of the swelling displacements. This discrepancy is attributed to the high permeability used in the analysis which prevents the generation of a deep desiccation zone (i.e., a drier initial state before construction). The permeability also affects the swelling rate, as it determines the time scale between recharge at the boundary and re-saturation in the dry region. More representative predictions are required to fully assess the model's capabilities after addressing the convergence difficulties encountered when dealing with low permeability and high suction conditions. Future work will also investigate the impact of building loading and stiffness on observed deformations through soil-structure interaction coupling.

ACKNOWLEDGEMENTS

This work is part of the first author's PhD research at the University of Oxford. Financial support provided by the Rhodes Trust, through the Rhodes Scholarship, to conduct this research is gratefully acknowledged.

REFERENCES

Alonso, E. E., & Navarro, V. (2005). Microstructural model for delayed deformation of clay: loading history effects. *Canadian Geotechnical Journal, 42*(2), 381-392. doi:10.1139/t04-097

Alonso, E. E., Vaunat, J., & Gens, A. (1999). Modelling the mechanical behaviour of expansive clays. *Engineering Geology, 54*(1), 173-183. doi:https://doi.org/10.1016/S0013-7952(99)00079-4

Biddle, P. G. (1983). Patterns of soil drying and moisture deficit in the vicinity of trees on clay soils. *Géotechnique, 33*(2), 107-126. doi:10.1680/geot.1983.33.2.107

Biddle, P. G. (2001). *Tree Root Damage to Buildings.* Paper presented at the Civil Engineering Conference (ASCE). Expansive clay soils and vegetation influence on shallow foundation: proceedings of Geo-Institute shallow foundation and soil properties committee sessions at the ASCE conference.

Cheney, J. E. (1988). 25 years' heave of a building constructed on clay, after tree removal. *Ground Engineering, 21*(5), 13-27.

Chung, S., & Austin, T. A. (1987). Modeling Saturated-Unsaturated Water Flow in Soils. *Journal of Irrigation and Drainage Engineering, 113*(2), 233-250. doi:doi:10.1061/(ASCE)0733-9437(1987)113:2(233)

Crilly, M. (2001). Analysis of a database of subsidence damage. *Structural Survey, 19*(1), 7-15. doi:10.1108/02630800110384185

Dixon, N., Crosby, C. J., Stirling, R., Hughes, P. N., Smethurst, J., Briggs, K., . . . Hudson, A. (2019). In situ measurements of near-surface hydraulic conductivity in engineered clay slopes. *Quarterly Journal of Engineering Geology and Hydrogeology, 52*(1). doi:10.1144/qjegh2017-059

Driscoll, R. (1983). The influence of vegetation on the swelling and shrinking of clay soils in Britain. *Géotechnique, 33*(2), 93-105. doi:https://doi.org/10.1680/geot.1983.33.2.93

El-Garhy, B., & Wray, W. (2006). *Investigation of a leaking water line beneath residential foundation on expansive soils.* Paper presented at the 4th International Conference on Unsaturated Soils, Carefree, Arizona.

Feddes, R. A., Kowalik, P., Kolinska-Malinka, K., & Zaradny, H. (1976). Simulation of field water uptake by plants using a soil water dependent root extraction function. *Journal of Hydrology, 31*(1), 13-26. doi:https://doi.org/10.1016/0022-1694(76)90017-2

Jones, L., Banks, V., & Jefferson, I. (2020). Swelling and shrinking soils. In D. P. Giles & J. S. Griffiths (Eds.), *Geological Hazards in the UK: Their Occurrence, Monitoring, and Mitigation - Engineering Group Working Party Report* (Vol. 29, pp. 223-242).

Mahfouf, J. F., & Noilhan, J. (1991). Comparative Study of Various Formulations of Evaporations from Bare Soil Using In Situ Data. *Journal of Applied Meteorology and Climatology, 30*(9), 1354-1365. doi:https://doi.org/10.1175/1520-0450(1991)030<1354:CSOVFO>2.0.CO;2

Mathias, S. A. (2023). *Hydraulics, Hydrology and Environmental Engineering*: Springer Cham.

Met Office, Hollis, D., McCarthy, M., Kendon, M., Legg, T., & Simpson, I. (2018). *HadUK-Grid gridded and regional average climate observations for the UK*. Retrieved from: https://catalogue.ceda.ac.uk/uuid/4dc8450d889a491ebb20e724debe2dfb/

Murphy, C., Wilby, R. L., Matthews, T., Horvath, C., Crampsie, A., Ludlow, F., . . . Jobbova, E. (2020). The forgotten drought of 1765–1768: Reconstructing and re-evaluating historical droughts in the British and Irish Isles. *International Journal of Climatology, 40*(12), 5329-5351. doi:https://doi.org/10.1002/joc.6521

Navarro, V., Asensio, L., De la Morena, G., Pintado, X., & Yustres, Á. (2015). Differentiated intra- and inter-aggregate water content models of mx-80 bentonite. *Applied Clay Science, 118*, 325-336. doi:https://doi.org/10.1016/j.clay.2015.10.015

Nelson, J. D., Overton, D. D., & Durkee, D. B. (2001). *Depth of Wetting and the Active Zone.* Paper presented at the Civil Engineering Conference (ASCE). Expansive clay soils and vegetation influence on shallow foundation: proceedings of Geo-Institute shallow foundation and soil properties committee sessions at the ASCE conference., Houston, Texas.

Norrish, K. (1954). The swelling of montmorillonite. *Discussions of the Faraday Society, 18*, 120-134. doi:10.1039/df9541800120

Nowamooz, H., Mrad, M., Abdallah, A., & Masrouri, F. (2009). Experimental and numerical studies of the hydromechanical behaviour of a natural unsaturated swelling soil. *Canadian Geotechnical Journal, 46*(4), 393-410. doi:10.1139/t08-127

Reeve, M. J., Hall, D. G. M., & Bullock, P. (1980). The effect of soil composition and environmental factors on the shrinkage of some clayey British soils. *Journal of Soil Science, 31*(3), 429-442. doi:https://doi.org/10.1111/j.1365-2389.1980.tb02092.x

van Genuchten, M. T. (1980). A Closed-form Equation for Predicting the Hydraulic Conductivity of Unsaturated Soils. *Soil Science Society of America Journal, 44*(5), 892-898. doi:https://doi.org/10.2136/sssaj1980.03615995004400050002x

Vrugt, J. A., van Wijk, M. T., Hopmans, J. W., & Šimunek, J. (2001). One-, two-, and three-dimensional root water uptake functions for transient modeling. *Water Resources Research, 37*(10), 2457-2470. doi:https://doi.org/10.1029/2000WR000027

Wang, G., & Wei, X. (2015). Modeling swelling–shrinkage behavior of compacted expansive soils during wetting–drying cycles. *Canadian Geotechnical Journal, 52*(6), 783-794. doi:10.1139/cgj-2014-0059

Wullschleger, S. D., Meinzer, F. C., & Vertessy, R. A. (1998). A review of whole-plant water use studies in tree. *Tree Physiology, 18*(8-9), 499-512. doi:10.1093/treephys/18.8-9.499